INSTITUTE OF PLASMA PHYSICS

NAGOYA UNIVERSITY

RESEARCH REPORT

NAGOYA, JAPAN

MAGNETOHYDRODYNAMIC INSTABILITIES IN A STELLARATOR

K. Matsuoka, K. Miyamoto, K. Ohasa and M. Wakatani

IPPJ-287 May 1977

Further communication about this report is to be sent to the Research Information Center, Institute of Plasma Physics, Nagoya University, Nagoya 464, Japan.

ABSTRACT

Numerical studies of stability on kink and resistive tearing modes in a linear stellarator are presented for various current profiles and helical fields. In the case of an $\ell = 2$ helical field, a magnetic shear vanishes and the stability diagram is given by the straight lines with $\iota^{\sigma} + \iota^{\delta} = \text{const.}$, where ι^{σ} is a rotational transform due to the plasma current and ι^{δ} is due to the helical field. In the $\ell = 2$ stellarator with $\iota^{\delta} > 0.5$, the m.h.d. stability against kink and tearing modes is improved compared with that in tokamaks.

While an $\ell = 3$ helical component exists, the magnetic shear plays an important role in the stability properties. The stability diagrams become fairly complex; however, they can be explained by properties of the Euler equation. It should be noted that the internal kink modes become more unstable than in tokamaks by the $\ell = 3$ helical field.

1. INTRODUCTION

Kink instabilities in a stellarator configuration have been studied theoretically by many authors [1,2]. Johnson et al. reduced the energy integral for fields represented by the stellarator expansion and obtained stability diagrams on kink modes when ohmic heating current has a uniform distribution.

Sinclair et al. generalized the earlier theoretical work on kink instabilities and presented a series of experimental results in the model C stellarator [3]. They calculated stability diagrams on kink modes numerically in the case of various profiles of plasma currents and helical fields. However, they did not notice the internal kink mode with $m = 1$ and $n = 1$ which may be observed as a precursor oscillation of internal disruption in tokamaks [4]. We will show that the internal kink mode in a stellarator with an $\ell = 3$ helical field is more unstable than in tokamaks.

The effect of finite resistivity on magnetohydrodynamic (m.h.d.) instabilities in a stellarator has been discussed by Johnson et al. [5]. Sinclair et al. also presented stability diagrams on the tearing mode analytically in the case of the uniform ohmic heating current [3]. It is considered that tearing modes make magnetic islands and deteriorate plasma confinement in tokamaks. In stellarators stability on tearing modes is not well known. We will calculate stability diagrams on tearing modes for various current profiles, following the method given by Furth et al. [6].

Recent experimental results on WVIIA stellarator show that no disruption of the current has been observed, even at $\iota = \iota^{\sigma} + \iota^{\delta} = 0.8$ at the edge of the plasma column and the m.h.d. stability may be improved

by the $\ell = 2$ helical field [7]. In the L-2 stellarator the $m = 1$ and $n = 1$ m.h.d. oscillation is observed for $\iota(0) \simeq 1$ [8]. In order to interpret these experimental results, more detailed stability diagrams on kink and tearing modes should be required.

In this paper we present detailed stability diagrams on the kink and resistive tearing mode in stellarators of various radial profiles of ohmic heating currents and helical fields by numerical calculations of the Euler equation.

2. COMPUTATION OF STABILITY DIAGRAMS

We treat a pressureless plasma in a linear stellarator with ohmic heating current. We neglect toroidal effects except the periodicity of length $L = 2\pi R$. In this paper, current driven kink modes and tearing modes are considered, since these non-localized instabilities are crucial for plasma confinement. We introduce three models corresponding to increasingly peaked current distributions:

flattened model: $$j_z(r) = j_0 \left(1 - \frac{r^6}{a^6}\right), \qquad (1)$$

parabolic model: $$j_z(r) = j_0 \left(1 - \frac{r^2}{a^2}\right), \qquad (2)$$

peaked model: $$j_z(r) = j_0 \left(1 - \frac{r^2}{a^2}\right)^4, \qquad (3)$$

where a is the minor radius of the current channel, j_0 the current density at the center of the plasma column. These configurations are shown in Fig.1. The external region from $r = a$ to $r = b$ is a vacuum region, where b is the wall radius.

A helical field is considered to produce only the rotational trans-

form angle $\iota^{\delta}(r)$ and the following cases are calculated:

$$\ell=2: \qquad \iota^{\delta}(r)=\iota_0^{\delta}\ , \tag{4}$$

$$\ell=2+\ell=3: \qquad \iota^{\delta}(r)=\iota_0^{\delta}\left(0.286+0.714\left(\frac{r}{a}\right)^2\right), \tag{5}$$

$$\ell=3: \qquad \iota^{\delta}(r)=\iota_0^{\delta}\left(\frac{r}{a}\right)^2, \tag{6}$$

where ι_0^{δ} is the rotational transform angle at the surface of the plasma column. Helical fields given by Eqs.(4), (5) and (6) correspond to those of WVIIA [7] and JIPP T-II [9] stellarators, L-2 stellarator with the short pitch ℓ = 2 helical coil [8] and CLEO stellarator [10], respectively.

Stability diagrams are obtained from the energy integral which is reduced to

$$2\delta W=\frac{8\pi^2}{k}\left\{\int_0^a r\,dr\left[\left(\frac{d\psi}{dr}\right)^2+\frac{\alpha}{r^2}\psi^2\right]-\frac{1}{a}\frac{d}{dr}\left(r^2\iota^{\sigma}\right)\frac{\psi^2}{\nu}\Big|_{r=a}\right.$$
$$\left.+\,m\psi^2(a)\,\frac{1+(a/b)^{2m}}{1-(a/b)^{2m}}\right\}, \tag{7}$$

where

$$\psi=\frac{krB_0}{2}\nu\xi\ ,$$

$$\nu=-\frac{2\pi n}{m}+\iota^{\sigma}(r)+\iota^{\delta}(r)\ ,$$

$$\alpha=m^2+\frac{1}{r\nu}\frac{d}{dr}\left(r^3\frac{d\iota^{\sigma}}{dr}\right)+\frac{4\pi^2 rB_0 J^{\beta}V''_{vac.}}{k\nu^2}\ ,$$

$$V''_{vac.}=\sum_i\frac{h_i}{2\pi\ell_i r^3 B_0^2}\frac{d(r^4\iota_i^{\delta})}{dr}\ .$$

Here ξ denotes the radial component of the plasma displacement. This expression is obtained for fields represented by the stellarator expansion. In Eq.(7) several terms that can make negative contributions of order $(kr/m)^2$ are neglected, since $kr << m$ is available for stellarators. The second term in Eq.(7) vanishes in our case, so that the plasma current falls to zero at the surface $r = a$. The term containing J^β in α also vanishes for a pressureless plasma, since this term denotes a diamagnetic effect.

First we consider the stability criterion of kink modes. We follow the analysis given by Newcomb [11]. From the energy integral of Eq.(7), we reduce the Euler equation to

$$\frac{d}{dr}\left(r\frac{d\psi}{dr}\right) - \frac{\alpha}{r}\psi = 0 . \qquad (8)$$

Equation (8) is integrated numerically in independent subintervals of a given helical equilibrium. The solution of Eq.(8) is given by $\psi \sim r^m$ near the origin. We integrate outward from the center $r = 0$ to the next singular point in the plasma. When there is no singular point inside the plasma, integration is made to the wall without taking account of singular points in the vacuum. At the plasma surface ψ and ψ' are continued to the analytical solution in the vacuum, that is, $\psi = Ar^m + Br^{-m}$. When there is one singular point inside the plasma, the integration is made in the two regions, $[0, r_s]$ and $[r_s, b]$, where r_s denotes the singular point. The latter integration is made inward from the wall with the boundary condition $\psi(b) = 0$. When several singular points exist in the plasma region, we follow the theorem by Newcomb. Near the singular point inside the plasma small solution ψ behaves such that $\psi = |r - r_s|$ and $\psi' = 1$. By these initial conditions the Euler equation is solved from the one singular point to the other singular point. The helical equilibrium is unstable against

the kink mode if ψ passes through zero in any independent subintervals.

We also consider tearing modes when the singular point exists in the plasma region. The stability criterion for the tearing mode is determined by the difference Δ' in the logarithmic derivative of ψ [5]:

$$\Delta' = \frac{d}{dr}(\psi_2 - \psi_1) \Big/ \psi(r_s) \quad , \tag{9}$$

where ψ_1 and ψ_2 are the solutions of the Euler equation in the respective subintervals $r < r_s$ and $r > r_s$ with the condition $\psi_1(r_s) = \psi_2(r_s)$. If this difference is greater than zero, the helical equilibrium is unstable against the tearing mode.

The parameters used in this calculation are as follows: a = 1 (the length is normalized by the plasma radius), b = 1.44 and 3.0, R = 20, k = 0.05 (this corresponds to n = 1), B_0 = 1.0. That b/a = 1.44 corresponds to the dimension of the JIPP T-II stellarator [12]. Since terms of the order of $(kr/m)^2$ are neglected, we restrict ourselves to the illustrative value k = 0.05, which does not appear explicitly in the Euler equation. The stability diagrams are obtained in the $(\iota_0^\sigma, \iota_0^\delta)$ plane, where both the rotational transform at the plasma surface ι_0^σ and ι_0^δ extend from zero to one.

3. STABILITY OF VARIOUS PROFILES OF PLASMA CURRENTS AND HELICAL FIELDS

Stability diagrams of the ℓ = 2 helical field are shown in Fig.2. The region of the m = 1 external kink modes which are unstable due to the singular point in vacuum is almost independent of the current profile. The m = 2 and m = 3 external kink modes are stabilized according to increasingly peaked current distributions and especially in the

case of the peaked current given in Eq.(3) the modes are completely stabilized. On the other hand the m = 2 and m = 3 tearing modes are unstable for $\iota_0^\delta < 0.5$ even in the peaked model. While the stellarator expansion is used in the energy integral, these tendency is similar to the stability analyses of tokamak by Shafranov [13]. The unstable region of the m = 1 external kink mode with zero ι^δ (i.e., tokamak) is given by

$$(a/b)^2 < 2\pi n/\iota_0^\sigma < 1 \qquad (10)$$

The Euler equation of Eq.(8) can be shown in terms of ξ as follows:

$$(r^3\nu^2\xi')' - \{(m^2-1)r\nu^2 - (3r\iota^{\delta\prime} + r^2\iota^{\delta\prime\prime})r\nu\}\xi = 0, \qquad (11)$$

where the prime denotes the derivative with respect to r. For the $\ell = 2$ helical field, Eq.(11) is reduced to

$$(r^3\nu^2\xi')' = (m^2-1)r\nu^2\xi, \qquad (12)$$

Since both $\iota^{\delta'}$ and $\iota^{\delta''}$ are equal to zero. This equation is equivalent to the one of the tokamak within our assumptions used here. For the $\ell = 2$ helical field the m = 1 internal kink mode is marginally stable, since we have neglected the pressure term and terms of the order of $(kr/m)^2$ which make negative but small contributions to the energy integral. From Eq.(11) the derivative of ξ is given by

$$\xi' = \frac{1}{r^3\nu^2}\int^r \{(m^2-1)r\nu^2 - (3r\iota^{\delta\prime} + r^2\iota^{\delta\prime\prime})r\nu\}\xi\, dr. \qquad (13)$$

The solution of the Euler equation for the m = 1 mode is given by ξ = const. near the origin. From Eq.(13) the solution ξ of the m = 1 internal kink mode has its derivative of zero for $\iota^{\delta'} = \iota^{\delta''} = 0$ and remains constant from the origin

to the singular point. If we take account of the inertia term $\rho\omega^2$ and terms of order of $(kr)^2$ in the energy integral, ξ falls to zero at the singular point and remains zero to the wall. This means that the m = 1 internal kink mode is marginally stable for the ℓ = 2 helical field [14].

Figures 3 and 4 show the stability diagrams with the finite component of the ℓ = 3 helical field. The stability diagrams of the ℓ = 2 + ℓ = 3 helical field are essentially determined by the ℓ = 3 helical field.

It is seen from Eq.(11) that the finite component of the ℓ = 3 helical field has stabilizing or destabilizing effects on the stability of the kink mode, depending on the value of the coefficient of ξ. For the m = 1 kink mode Eq.(11) is reduced to

$$\left(r^3 \nu^2 \xi'\right)' = -\left(3 r \iota^{\delta'} + r^2 \iota^{\delta''}\right) r \nu \xi \,, \qquad (14)$$

where $\iota^{\delta'}$ and $\iota^{\delta''}$ are always positive.

The external kink mode with no singular point in the range of $0 < r < b$ can be unstable. In the region of horizontally striped areas by dashed lines, ν remains positive and the right hand side of Eq.(14) has a negative value if ξ is positive. From Eq.(14) the solution ξ for the m = 1 external kink mode has a negative derivative of ξ and leads to zero crossing, i.e., instability of the mode even without the singular point. The m = 1 external kink mode with the singular point in the vacuum is explained by the same reason. The unstable m = 1 'external kink mode' with the singular point inside the plasma is shown in the figures of the flattened and parabolic current profiles. We consider this instability is equivalent to the external kink mode, since the surface of the plasma column is perturbed. In this case ν is negative and ξ has a positive derivative in the range of $0 < r < r_s$. Instability does not occur from consideration of the behavior of ξ in this range.

In the range of $r_s < r < b$, however, ν is positive and $\xi' < 0$. Then integrating Eq.(14) from $r = r_s$ with a small solution near r_s, i.e., ξ = const., we can see ξ crosses zero in the subinterval $[r_s, b]$ for large $\iota^{\delta'}$ and $\iota^{\delta''}$.

For the helical equilibrium of a finite $\ell = 3$ helical field, the $m = 1$ internal kink mode occurs to be unstable for the same reason of negative derivative of ξ. When ι_0^{δ} is zero the mode is marginally stable in accordance with the case of the $\ell = 2$ helical field.

The $m = 2$ and $m = 3$ internal kink modes also can become unstable if the condition

$$(m^2-1)\nu < 3r\iota^{\delta'} + r^2\iota^{\delta''} \qquad (15)$$

is satisfied. From the above condition it is necessary for the modes to be unstable that the rotational transform angle associated with the $\ell = 3$ helical field is larger than some critical value as shown in the figures. The modes are more unstable when ι_0^{δ} increases.

Wall effect is shown in Fig.5 for the parabolic current profile and the various helical fields. Comparing with Figs.2-4 it is seen from Fig.5 that wall stabilization is effective on the $m = 1$ and $m = 2$ external kink modes and less effective on the $m = 3$ external kink and the internal kink modes. The results are similar to those of tokamak given by Shafranov [13]: external kink modes are stabilized by the wall as m decreases.

The unstable ranges of the $m = 2$ and $m = 3$ tearing modes as a function of r_s are shown in Fig.6 for various current profiles and the $\ell = 3$ helical field. The tearing modes become more unstable according to more flattened current profiles. When $\iota_0^{\delta} = 0$, values of Δ' are same as the case of the $\ell = 2$ helical field and this quantity is independent of the rotational transform associated with the $\ell = 2$ helical field. In Fig.6(b) the effect of the wall location is shown when $\iota_0^{\delta} = 0$. In the case of the $m = 3$ mode, the effect is too slight to be seen on

the graph. The constant ψ approximation [15] may not be applicable for the m = 1 tearing mode appearing in the flattened and parabolic current profiles, since the finite-resistivity region is not assumed to be very thin compared with the radius.

4. CONCLUDING RAMARKS

We obtain stability diagrams on the kink and tearing modes for three current profiles and three cases of linear stellarator configurations. These diagrams will be useful in investigating m.h.d. properties of stellarators with an ohmic heating current. More detailed studies including plasma pressure and toroidal effects are remained for the future research.

REFERENCES

[1] JOHNSON, J.L., OBERMAN, C.R., KULSRUD, R.M., FRIEMAN, E.A., Phys. Fluids 1 (1958) 281.

[2] KRUSKAL, M.D., JOHNSON, J.L., GOTTLIEB, M.B., GOLDMAN, L.M., Phys. Fluids 1 (1958) 421.

[3] SINCLAIR, R.M., YOSHIKAWA, S., HARRIES, W.L., YOUNG, K.M., WEIMER, K.E., JOHNSON, J.L., Phys. Fluids 8 (1965) 118.

[4] VON GOELER, S., STODIEK, W., SAUTHOFF, N., Phys. Rev. Letters 33 (1974) 1201.

[5] JOHNSON, J.L., GREENE, J.M., COPPI, B., Phys. Fluids 6 (1963) 1169.

[6] FURTH, H.P., RUTHERFORD, P.H., SELBERG, H., Phys. Fluids 16 (1973) 1054.

[7] WVIIA TEAM, Plasma Physics and Controlled Nuclear Fusion Research (Proc. 6th Int. Conf., Berchtesgaden, 1976) IAEA-CN-35/D2.

[8] AKULINA, D.K. et al., ibid., IAEA-CN-35/D5.

[9] FUJITA, J. et al., ibid., IAEA-CN-35/D3.

[10] ATKINSON, D.W. et al., ibid., IAEA-CN-35/D1.

[11] NEWCOMB, W.A., Ann. Phys. 10 (1960) 232.

[12] Project JIPP T-II, IPPJ-205 (Inst. Plasma Phys., Nagoya Univ., Japan, 1974)

[13] SHAFRANOV, V.D., Sov. Phys. Tech. Phys. 15 (1970) 175.

[14] ROSENBLUTH, M.N., DAGAZIAN, R.Y., RUTHERFORD, P.H., Phys. Fluids 16 (1973) 1894.

[15] FURTH, H.P., KILEEN, J., ROSENBLUTH, M.N., Phys. Fluids 6 (1963) 459.

FIGURE CAPTIONS

Fig.1. Profiles of ohmic heating currents $j_z(r)$ and rotational transform angles $\iota^{\sigma}(r)$ associated with the plasma current in arbitrary units. Solid lines refer to the current, dashed ones to the rotational transform angle. 1: flattened model, 2: parabolic model, 3: peaked model.

Fig.2. Stability diagrams for the $\ell = 2$ helical field. (a): flattened model, (b): parabolic model, (c): peaked model. Horizontally striped areas and dotted ones are unstable regions against an external kink mode and a resistive tearing mode, respectively. The regions into which singular points fall are shown for the $m = 1$, $n = 1$ diagram.

Fig.3. Stability diagrams for the $\ell = 2 + \ell = 3$ helical field. (a): flattened current, (b): parabolic current, (c): peaked current. Horizontally striped areas by dashed lines are unstable regions against an external kink mode which has no singular point in the region $0 < r < b$. Vertically striped areas are unstable regions against an internal kink mode. There are more than one singular points where the areas indicating the position of r_s overlap each other.

Fig.4. Stability diagrams for the $\ell = 3$ helical field. (a): flattened current, (b): parabolic current, (c): peaked current.

Fig.5. Stability diagrams for the parabolic current and the wall position of $b/a = 3$. (a): $\ell = 2$, (b): $\ell = 2 + \ell = 3$, (c): $\ell = 3$. External kink modes of $m = 1$ and $m = 2$ extend their unstable regions. The area of the unstable $m = 3$ mode changes little.

Fig.6. Values of Δ' as a function of r_s in the case of the $\ell = 3$ helical field. (a): flattened current, (b): parabolic current, (c): peaked current. Solid lines refer to the $m = 2$ mode, dashed ones to the $m = 3$ mode. The effect of the wall location is shown for the parabolic current profile with $\iota_o^\delta = 0$.

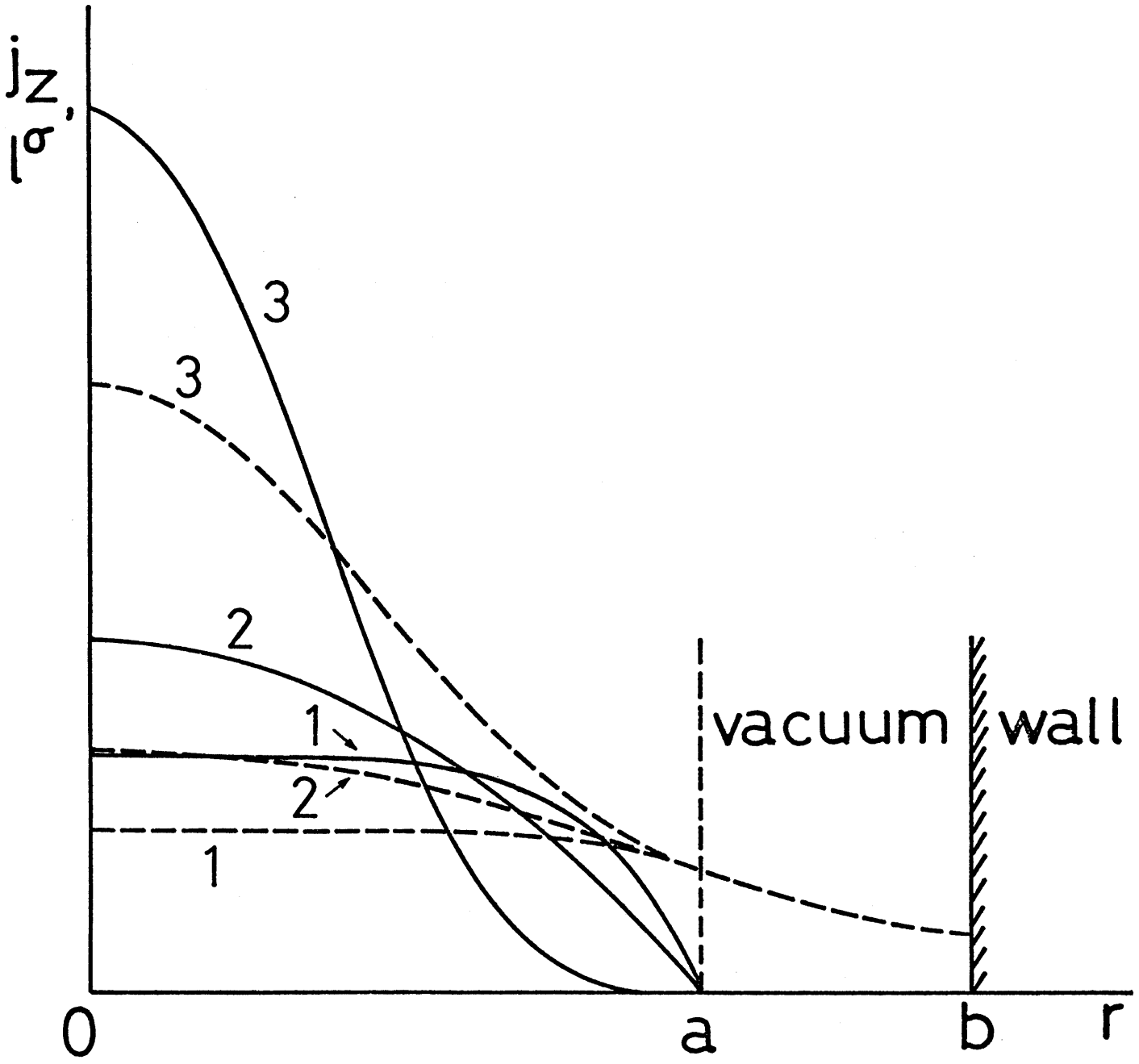

Fig.1

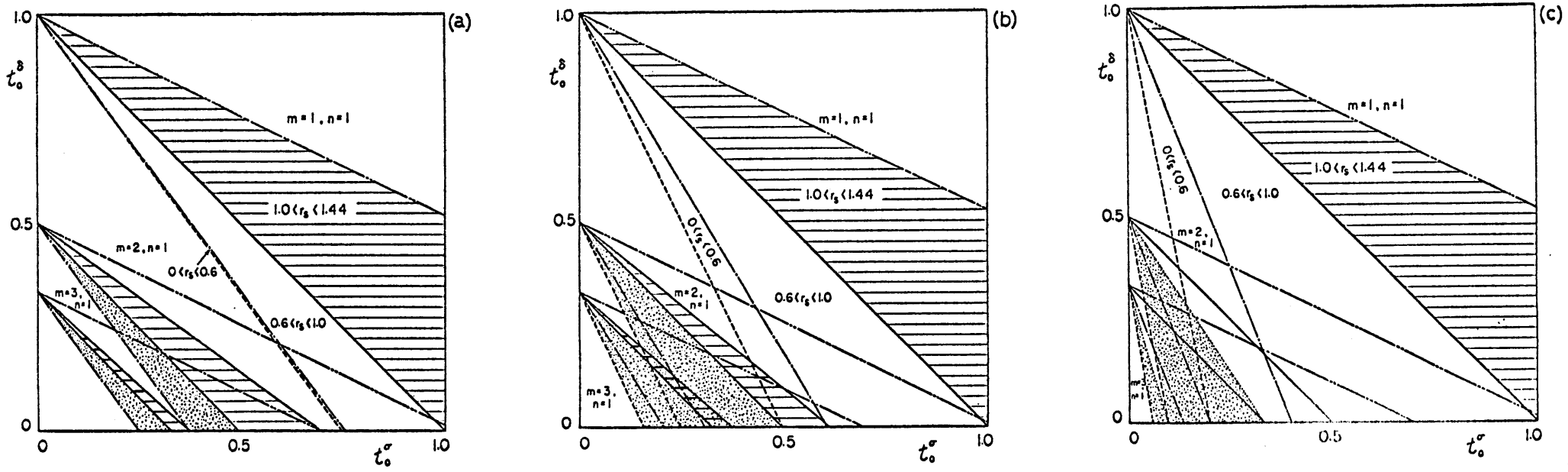
(a)
(b)
(c)
1.0
0.5
0
t_o^δ
t_o^σ
m=1, n=1
1.0<r_s<1.44
m=2, n=1
0<r_s<0.6
0.6<r_s<1.0
m=3, n=1

Fig. 2

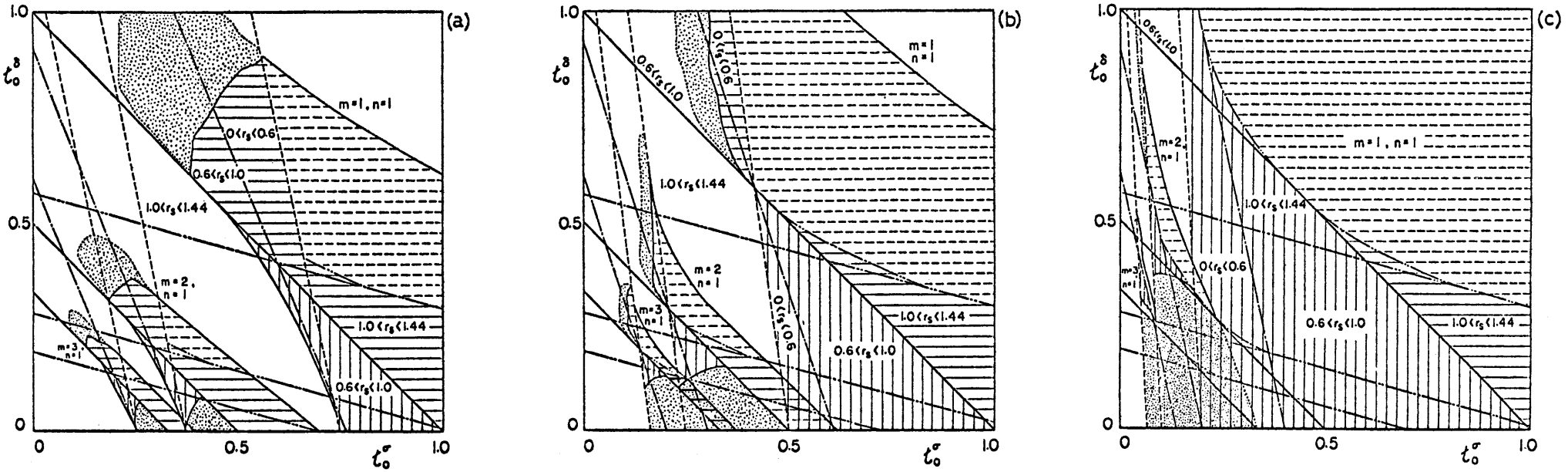
(a)
(b)
(c)
1.0
0.5
0
t_0^δ
t_0^σ
m=1, n=1
m=2, n=1
m=3, n=1
0<r_s<0.6
0.6<r_s<1.0
1.0<r_s<1.44

Fig.3

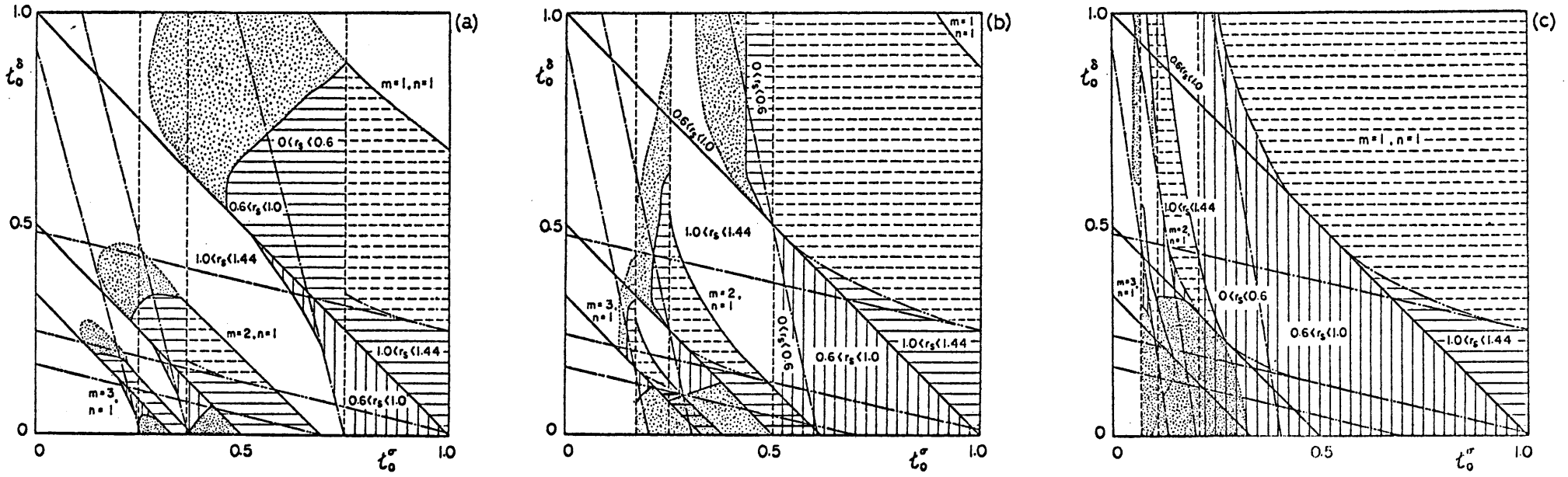
(a)
1.0
0.5
0
t_0^δ
t_0^σ
m=1, n=1
0<r_s<0.6
0.6<r_s<1.0
1.0<r_s<1.44
m=2, n=1
m=3, n=1
(b)
m=1 n=1
0.6<r_s<1.0
0<r_s<0.6
1.0<r_s<1.44
m=2, n=1
m=3, n=1
(c)
0.6<r_s<1.0
m=1, n=1
1.0<r_s<1.44
m=2 n=1
m=3 n=1
0<r_s<0.6
0.6<r_s<1.0
1.0<r_s<1.44

Fig. 4

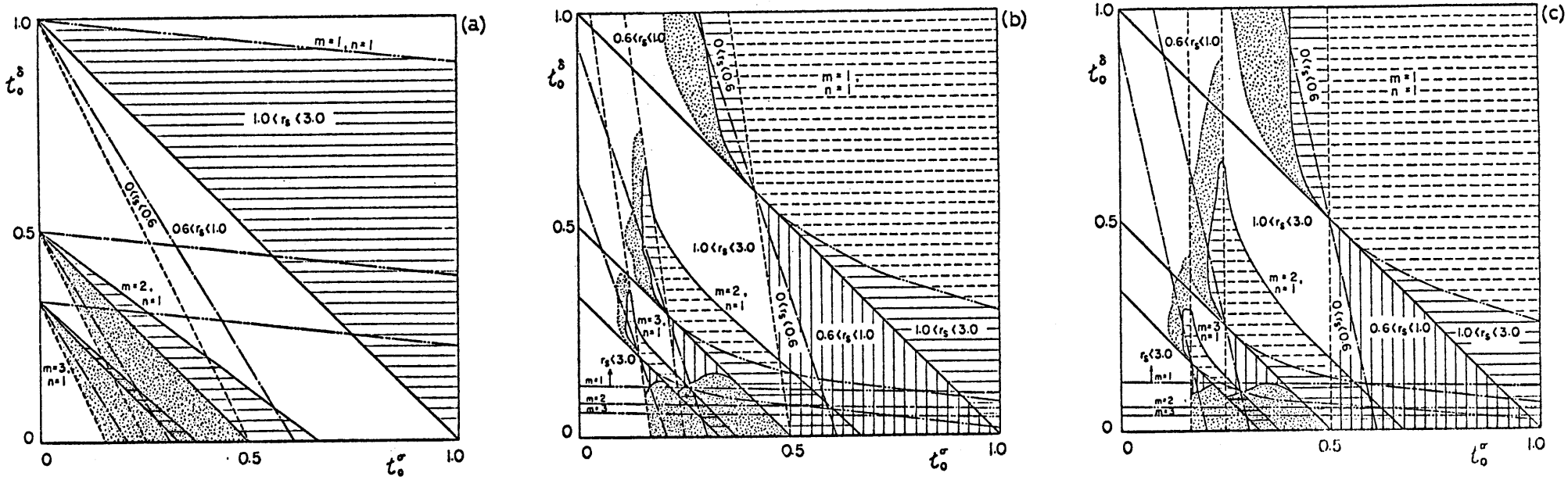
(a)
(b)
(c)
1.0
0.5
0
t_0^δ
t_0^σ
m=1, n=1
1.0<r_s<3.0
0<r_s<0.6
0.6<r_s<1.0
m=2, n=1
m=3, n=1
r_s<3.0
m=1
m=2
m=3

Fig.5

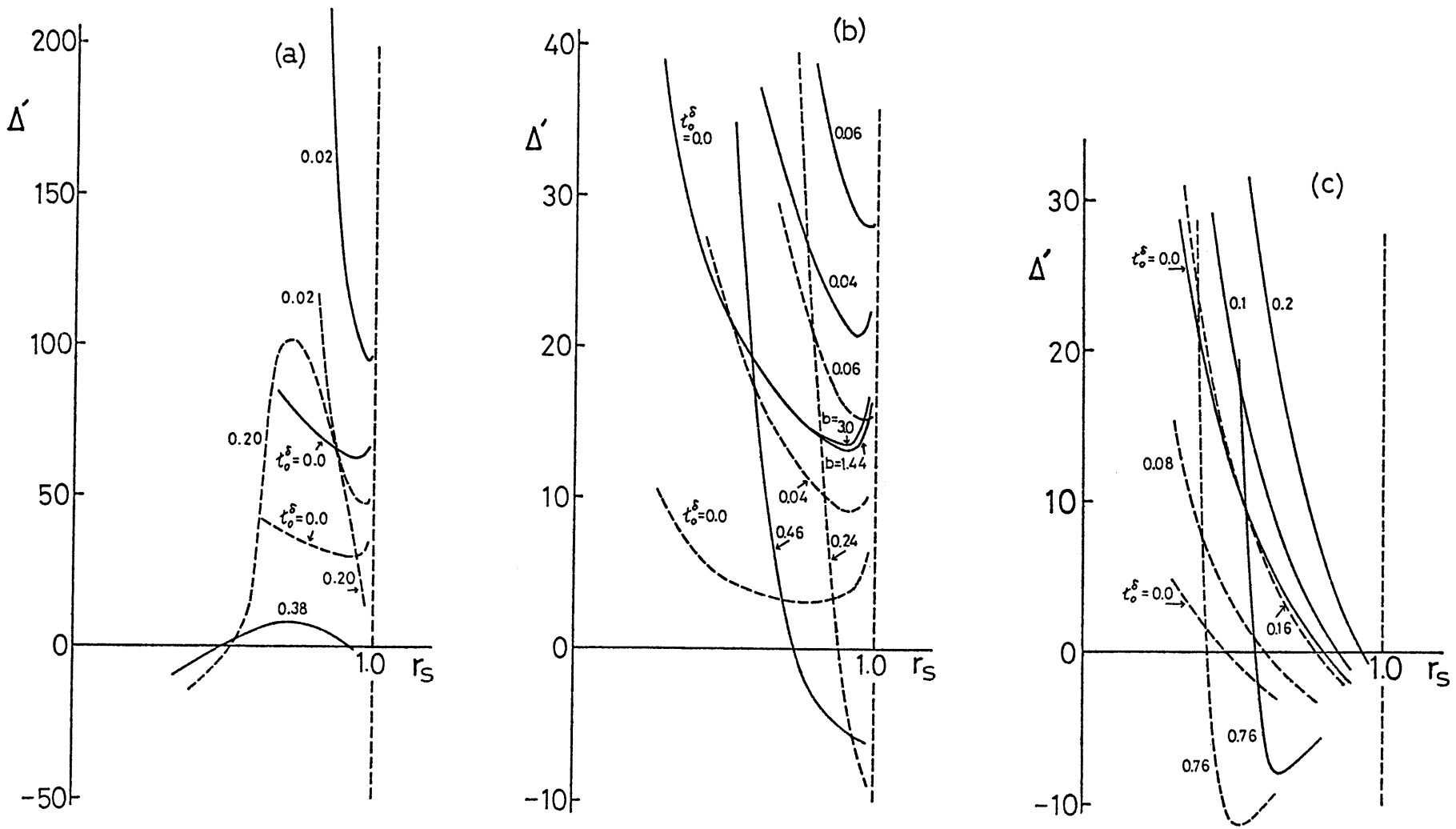
(a)
(b)
(c)
Δ′
r_s
1.0
200
150
100
50
0
-50
40
30
20
10
-10
0.02
0.20
0.38
0.04
0.06
0.24
0.46
0.08
0.1
0.2
0.16
0.76
b=3.0
b=1.44
t_o^δ=0.0

Fig.6